The $S_1Y_Z^\bullet$ Metalloradical EPR Signal of Photosystem II Contains Two Distinct Components That Advance Respectively to the Multiline and $g = 4.1$ Conformations of S_2[†]

George Sioros, Dionysios Koulougliotis, George Karapanagos, and Vasili Petrouleas*

Institute of Materials Science, NCSR Demokritos, 153 10 Aghia Paraskevi Attikis, Greece

Received June 20, 2006; Revised Manuscript Received September 21, 2006

ABSTRACT: The S_2 state of the oxygen-evolving complex (OEC) of photosystem II is heterogeneous, exhibiting two main EPR spectral forms, the multiline and the $g = 4.1$ signal. It is not clearly established whether this heterogeneity develops during the S_1 to S_2 transition or is already present in the precursor states. We have compared the spectra of the $S_1Y_Z^\bullet$ intermediate, obtained by visible light excitation (induction of charge separation) of the S_1 state at liquid He temperatures, $(S_1Y_Z^\bullet)_{vis}$, or by near-infrared (NIR) light excitation of the S_2 state (utilization of the unusual property of the Mn cluster to act as an oxidant of Y_z when excited by NIR), $(S_1Y_Z^\bullet)_{NIR}$. The decay kinetics of the $(S_1Y_Z^\bullet)_{vis}$ spectrum at 11 K was also studied by the application of rapid-scan EPR. The two spectra share in common a signal with a characteristic feature at $g = 2.035$, but the $(S_1Y_Z^\bullet)_{vis}$ spectrum contains in addition a fast decaying component 26 G wide. The analysis of the surface of the rapid-scan spectra yielded 270 ± 35 and 90 ± 15 s for the respective half-times of the two components of the $(S_1Y_Z^\bullet)_{vis}$ spectrum at 11 K. $(S_1Y_Z^\bullet)_{vis}$ advances efficiently to S_2 when annealed at 200 K; notably the $g = 2.035$ signal advances to the multiline while the 26 G component advances to the $g = 4.1$ conformation. The "26 G" component is absent or very small, respectively, in thermophilic cyanobacteria or glycerol-containing spinach samples, in correlation to vanishing or very small amounts of the $g = 4.1$ component in the S_2 spectrum. The results validate the assignment of $S_1Y_Z^\bullet$ to a true S_1 to S_2 intermediate and imply that the heterogeneity observed in S_2 is already present in S_1. Tentative valences are assigned to the individual Mn ions of the OEC in the two heterogeneous conformations of S_1.

Photosystem II (PSII),[1] a membrane−protein complex of green plants, algae, and cyanobacteria, catalyzes a ubiquitous reaction, the oxidation of water to molecular oxygen. This is a four-step process, activated by sequential excitation of P_{680}, a specialized chlorophyll moiety, by four photons. Following each photon excitation an electron is transferred from P_{680} to a terminal electron acceptor, an iron−quinone complex, while a Mn cluster acts as the electron donor to P_{680}^+ via a redox-active tyrosine denoted Tyr Z or Y_Z. The Mn cluster (believed to be tetranuclear) with its cofactors, especially Ca^{2+}, comprises what is called the oxygen-evolving complex (OEC). The OEC undergoes four oxidative state transitions, S_0-S_1, ..., $S_3-(S_4)S_0$ during the sequential absorption of the four photons by P_{680}. The S-state transitions are accompanied by the loss of a total of four protons from bound water. Oxygen evolves during the S_3 to S_0 transition, the S_4 being a transient state (see refs *1*−*3* for reviews).

EPR spectroscopy has provided valuable information on the electronic properties of the OEC in the various S states. The most extensively studied state is S_2. S_2 is well-known for exhibiting heterogeneity. Two main EPR spectral forms are observed in the most commonly used preparations, the multiline (*4*) and the $g = 4.1$ signal (*5*, *6*; reviewed in ref *7*). These correspond to different spin ground states of the Mn cluster (*7*) attributed to different valence arrangements (*8*; see also ref *9*). It is not clearly established whether this heterogeneity develops during the S_1 to S_2 step or is already present in the precursor states. Parallel-mode EPR studies of the difficult to probe S_1 state have indicated the presence of two different kinds of EPR signals: a broad signal at $g = 4.8$ (*10*, *11*) and a multiline signal at $g = 12$ (*12*). To the best of our knowledge no one has reported the simultaneous detection of both signals in the same preparation. Recently, intermediates of almost all S-state transitions in oxygen-evolving preparations have been trapped at liquid helium temperatures and identified by EPR spectroscopy (*13*−*19*;

[†] Financial support of the program AKMWN of the Greek GSRT is kindly acknowledged.

* Corresponding author. Tel: +301 650-3344. Fax: +301 651-9430. E-mail: vpetr@ims.demokritos.gr.

[1] Abbreviations: PSII, photosystem II; OEC, oxygen-evolving complex; S states (S_0, ..., S_4), oxidation states of the OEC; Tyr Z or Y_Z and Tyr D or Y_D, the fast and slow tyrosine electron donors of PSII; signal II, the characteristic EPR signal of either of the two isolated tyrosine radicals; $(S_1Y_Z^\bullet)_{vis}$ and $(S_1Y_Z^\bullet)_{NIR}$, the metalloradical signals of the Tyr Z radical magnetically interacting with the Mn cluster in the S_1 state produced respectively by visible light excitation of S_1 or NIR excitation of S_2; Chl_Z and Car, a chlorophyll and carotene acting as electron donors in side pathways; pheo, the pheophytin primary electron acceptor of PSII; Q_A and Q_B, the primary and secondary plastoquinone electron acceptors of PSII; BBY membranes, thylakoid membrane fragments enriched in PSII; MES, 2-(*N*-morpholine)-ethanesulfonic acid; Chl, chlorophyll; PPBQ, *p*-phenylbenzoquinone; DMSO, dimethyl sulfoxide; NIR light, near-infrared light; EPR, electron paramagnetic resonance.

10.1021/bi061224i CCC: $37.00
Published on Web 12/13/2006

reviewed in ref *20*; see also ref *9* for the more recent trapping of the functional S_2 to S_3 intermediate). The intermediates have been assigned to Tyr $Z^\bullet$ magnetically interacting with the Mn cluster and are considered to be important for a number of reasons. They introduce EPR spectroscopy to the transient reactions accessible earlier only by fast optical spectroscopy. They provide an important tool to examine e^-/H^+ transfer reactions during the S-state transitions (*9*, *20*). They provide important information about the coupling of Tyr Z with the Mn cluster and, indirectly, about the magnetic properties of the Mn cluster itself (*18*). The latter information is important for states with no easily discernible EPR signatures, such as the S_1 state.

In the present paper we examine the spectral composition of the $S_1Y_Z^\bullet$ intermediate. This intermediate can be produced by visible light excitation of the S_1 state, $(S_1Y_Z^\bullet)_{vis}$ (*13*, *15*, *16*), or by near-infrared (NIR) excitation of the S_2 state, $(S_1Y_Z^\bullet)_{NIR}$ (*14*), at liquid helium temperatures. The EPR spectra at X-band frequencies contain a characteristic peak at $g = 2.035$, but the $g = 2$ region is not well resolved. The $(S_1Y_Z^\bullet)_{vis}$ spectra obtained at two frequencies, X and W band, were analyzed recently assuming an anisotropic ferromagnetic exchange interaction between the spin $S = {}^1/_2$ of the $Y_Z^\bullet$ radical and two low-lying spin multiplets of the Mn cluster, $S = 0$ and $S = 1$ (*18*). The analysis reproduced the major features of the spectra, but as was noted, an uncertainty remained in the $g = 2$ region. An inherent difficulty in achieving reliable spectral deconvolution in the $g = 2$ region is the presence of a large background signal contribution from oxidized tyrosine D, Tyr $D^\bullet$, and the accumulation during illumination of free radical contributions from less efficient side donors. We have examined the line shape of the $S_1Y_Z^\bullet$ intermediate both in spinach and in thermophilic, cyanobacterial PSII preparations and under conditions where Tyr D is oxidized or fully reduced. Flash illumination was applied in certain experiments in order to minimize oxidation of side donors (*15*). To obtain whole spectra kinetic images (2-D spectra evolution), a rapid-scan EPR technique was applied. The experiments revealed that the $(S_1Y_Z^\bullet)_{vis}$ spectrum contains, in addition to the common signal at $g = 2.035$, a fast decaying component centered at $g = 2.0$ with a width of 26 G. Extensive evidence is presented that the two components are the precursors of the multiline and the $g = 4.1$ conformations of S_2. The heterogeneity of S_2 is therefore already present in S_1. Tentative valence assignments on the Mn ions in the two conformations of S_1 are also made.

MATERIALS AND METHODS

PSII Sample Isolation. PSII-enriched thylakoid membranes were isolated from market spinach by standard procedures (*21*, *22*) with some modifications. Samples for EPR measurements were suspended in 0.4 M sucrose, 15 mM NaCl, 5 mM $MgCl_2$, and 40 mM MES, pH 6.5, at 6−8 mg of Chl/mL and stored in liquid nitrogen until use. Samples were dark adapted at 273 K for 1 h prior to the EPR measurements. In order to enhance the $S_1Y_Z^\bullet$ signal (*13*), the BBY membranes were supplemented with exogenous quinone, 0.75 mM duroquinone, or 0.75 mM PPBQ from stock solutions in DMSO. PSII preparations isolated from *Synechococcus elongatus* were a kind gift of Dr. A. Zouni (Berlin Technical University).

Ascorbate Reduction of Tyr D$^\bullet$. Tyr $D^\bullet$ was reduced by the addition of 10 mM sodium ascorbate and 0.3 mM DCPIP to samples diluted to 0.2 mg of Chl/mL. After 45 min of dark incubation on ice, the added chemicals were removed by repeated dilution and centrifugation.

Glycerol-treated samples were resuspended and washed twice in a buffer containing 50% glycerol, 15 mM NaOH, 5 mM $MgCl_2$, and 40 mM MES, pH 6.5, at 6−8 mg of Chl/mL.

Sample Illumination. Flash excitation of the samples was done with either of two studio photographic flash power supplies: one with a nominal power of 600 W and a pulse duration of 2.1 ms providing nearly saturating flashes or one with a 200 W nominal power and a pulse duration of 1.2 ms. Flashes at 11 K were given inside the EPR cavity. Heat artifacts were checked with the impurity $g = 4.3$ signal of samples in the S_1 state or with the stable EPR free radical signal of Tyr $D^\bullet$, signal II. Both signals show a strong variation with temperature at 11 K, while they are light insensitive. A small heat artifact was observed with the 600 W power supply causing a 3−4 s delay in the restoration of the EPR signal intensity, while no temperature artifact was observed with the 200 W power supply. The $S_1Y_Z^\bullet$ signals were recorded ∼15 s after the flash excitation. Samples were advanced to the S_2 state by illumination at 200 K for 4 min with a 360 W halogen projector lamp filtered with a saturated aqueous solution of $CuSO_4$. The same lamp was used for NIR excitation of the samples at 11 K. A 3 mm SCHOT RG715 NIR filter immersed in water was used in this case.

EPR Measurements. EPR measurements were obtained with an upgraded Bruker ER-200D spectrometer interfaced to a personal computer and equipped with an Oxford ESR 900 cryostat, an Anritsu MF76A frequency counter, and a Bruker 035M NMR gaussmeter. The perpendicular mode 4102ST cavity was used, and the microwave frequency was 9.41 GHz. Rapid-scan experiments were performed with the same spectrometer modified as follows. The Signal-Channel unit was replaced with an SR830 digital lock-in amplifier by Stanford Research. Data are recorded by a multifunction NI 6251 pci card by National Instruments (16 bit/1.25 MS/s) mounted on a personal computer running appropriate software in the LabView programing environment. Synchronization of the data acquisition with the magnetic field ramp produced by the Time Base unit is achieved by triggering the AD converter with a TTL pulse produced by the Time Base unit at the beginning of each scan. The minimum duration possible for each scan is 20 ms, and there is an additional delay of 20 ms between the scans. Scans of 2 s duration were employed in the present experiments.

Deconvolution of the Spectra and Determination of the $t_{1/2}$ Values. As described in the Results section, the $(S_1Y_Z^\bullet)_{vis}$ spectra contain two kinetically distinct components. Two methods were used for the deconvolution of the spectra.

(a) The kinetics of the more slowly decaying component at $g = 2.035$ is determined directly from the decay of the signal intensity at a field position where there is minimum overlap with other spectral components. The decay kinetics of the $g = 2.035$ signal is used in turn to normalize spectra at different times to the intensity of the $g = 2.035$ signal at $t = 0$ and obtain difference spectra, (spectrum at $t = 0$) minus (normalized spectrum at time t), that contain only the signal of the fast-decaying component. The peak to peak intensity

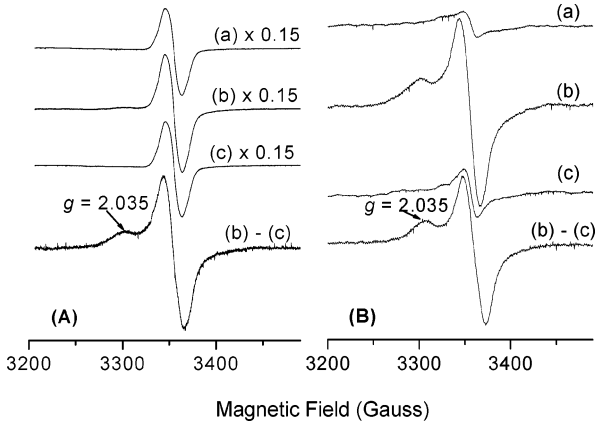

FIGURE 1: Production of the $(S_1Y_Z^{\bullet})_{vis}$ signal in PSII spinach preparations supplemented with duroquinone. (A) Samples with Tyr D naturally oxidized in the majority of centers. (B) Samples with Tyr D fully reduced by ascorbate treatment. The spectra were recorded after the following successive treatments: (a) dark adaptation for 1 h at 0 °C; (b) visible flash excitation at 11 K; (c) 30 min dark adaptation at 11 K. The lowest two difference spectra represent the $(S_1Y_Z^{\bullet})_{vis}$ signal in the two preparations. EPR parameters: microwave frequency, 9.41 GHz; modulation amplitude, 10 Gpp; microwave power, 115 mW; $T = 11$ K. The recording time of each spectrum was 50 s.

of the latter, derived by this method, evolves with time according to the following formula, obtained by simple mathematical manipulations and assuming single exponential decay of both components:

$$I_{fast}(t) = F(1 - e^{k_1 t}e^{-k_2 t})$$

Fitting of the data with this formula provides the value of the decay time $t_2 = 1/k_2$, based on the known decay time $t_1 = 1/k_1$ of the $g = 2.035$ component. F is a normalization factor.

(b) The experimental rapid-scan spectral surface was fitted to the formula:

$$A(B,t) = A_1(B)e^{-k_1 t} + A_2(B)e^{-k_2 t} + A_3(B)$$

where A is the signal intensity at field B and time t. The surface is assumed to be the convolution of two exponentially decaying EPR signals with field-dependent amplitudes A_1 and A_2 and respective decay rates $k_1 = 1/t_1$ and $k_2 = 1/t_2$ superimposed to a time-independent background spectrum A_3. The fitting with the above formula was done in the Matlab programing environment using the built-in function fminsearch.

RESULTS AND DISCUSSION

The $(S_1Y_Z^{\bullet})_{vis}$ Signal Induced by Visible Flash Excitation of Samples in the S_1 State with the Tyr D Oxidized or Fully Reduced. Figure 1 compares the production of the $(S_1Y_Z^{\bullet})_{vis}$ signal in (A) a spinach PSII sample with the majority of Tyr D naturally oxidized (typically 80% oxidized Tyr D) and (B) a similar sample with Tyr D fully reduced by treatment with ascorbate. The spectra have been recorded at high power (115 mW) to enhance the metalloradical features which do not saturate easily in contrast to Tyr D$^{\bullet}$ or other free radicals that are characterized by small $P_{1/2}$ values, of the order of 0.1 mW, and appear overly saturated under the present conditions. Large differences in the $g = 2$ region exist in the two sets of spectra due to the presence of the strong signal II contribution (the signal shape is distorted by the use of high power in these experiments) in the spectra in (A). To facilitate comparison, the spectra in (A) have been scaled down by the indicated factors. Taking into account these factors, the intensity of trace a in (B) is about 6% of the corresponding trace in (A). At 60 dB this proportion becomes smaller (spectra not shown). At the latter nonsaturating power the spectrum in (A) is overwhelmed by the spectrum of Tyr D$^{\bullet}$ while no signals above the noise level can be detected for the spectrum of sample B. It is concluded that the Tyr D$^{\bullet}$ level in (B) is vanishingly small [at most 1−3% of that in (A)], and the small $g = 2$ contributions in Figure 1B, spectrum a, are a mixture of the above and nonsaturating impurity species. Traces b show the spectra recorded immediately after visible flash excitation at 11 K. Traces c show the signal level 30 min after the flash, a time that is sufficient for the decay of the $(S_1Y_Z^{\bullet})_{vis}$ signal (*13*). The somewhat increased signal level compared to traces a is due to side donors such as carotenoids (*23*) that decay more slowly than the $(S_1Y_Z^{\bullet})_{vis}$ signal (*15*). These side donors, which are oxidized with low-quantum efficiency, are drastically minimized by the use of flash illumination but are not fully eliminated. The lowest traces in Figure 1 show the $(S_1Y_Z^{\bullet})_{vis}$ spectra as differences of the illuminated spectra minus the 30 min dark-adapted ones. This difference minimizes the contributions from stable side donors. The spectra are characterized by the $g = 2.035$ component (*13*) and an intense contribution centered at $g \sim 2$. The $(S_1Y_Z^{\bullet})_{vis}$ spectra in the two samples are practically superimposable except for small differences that are due to a variation of the relative abundance of the components that will be discussed in this paper. The similarity of the two spectra eliminates the possibility of artifacts due to a change of the relaxation properties of signal II (relaxation enhancement; *24*) upon formation of the $(S_1Y_Z^{\bullet})_{vis}$ state. Similar results are obtained by treatment with a low concentration of NO, which eliminates signal II by reversible binding to Tyr D$^{\bullet}$ (*25*, *26*).

Comparison of the $(S_1Y_Z^{\bullet})_{vis}$ Spectrum with the $(S_1Y_Z^{\bullet})_{NIR}$ Signal Induced by NIR Excitation of the S_2 state. Figure 2 compares the $(S_1Y_Z^{\bullet})_{vis}$ spectrum obtained in an ascorbate-treated spinach PSII preparation, spectrum a, with the $(S_1Y_Z^{\bullet})_{NIR}$ spectrum induced by NIR excitation of the S_2 state in the same preparation, spectrum b, or in a thermophilic, cyanobacterial preparation (*S. elongatus*), spectrum c. The latter two spectra are practically identical, but spectrum c will be used in further comparisons, as it has a better signal to noise ratio. Both the $(S_1Y_Z^{\bullet})_{vis}$ and the $(S_1Y_Z^{\bullet})_{NIR}$ spectra contain the $g = 2.035$ component as noted earlier (*14*) (the spectra have been normalized to approximately the same intensity of the $g = 2.035$ component), but significant differences can be observed in the central region. The difference (a) − (c) is a derivative signal approximately 25 G wide, the lowest spectrum.

Decay of the $(S_1Y_Z^{\bullet})_{vis}$ Spectrum. The comparison of the $(S_1Y_Z^{\bullet})_{vis}$ and $(S_1Y_Z^{\bullet})_{NIR}$ spectra in Figure 2 suggested that the $(S_1Y_Z^{\bullet})_{vis}$ spectrum contains two main components. We have searched for decay kinetic differences between the two by employing rapid scans. This method has the advantage that it provides full spectra at each time point and one can easily correct for drifts of the baseline and also examine for the simultaneous kinetic behavior of different parts of the

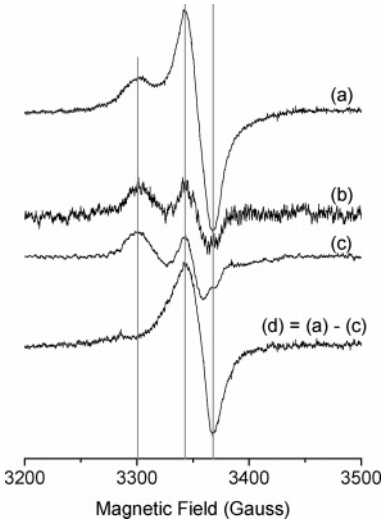

FIGURE 2: Comparison of the $(S_1Y_Z^\bullet)_{vis}$ spectrum in an ascorbate-treated spinach PSII preparation supplemented with duroquinone (a) with the $(S_1Y_Z^\bullet)_{NIR}$ spectrum induced by NIR excitation of the S_2 state in the same preparation, spectrum (b), or in *S. elongatus*, spectrum (c). The spectra have been normalized to approximately the same intensity of the $g = 2.035$ component. Spectrum (d) is the difference (a) − (c). The background spectra obtained after full decay of the $g = 2.035$ component were subtracted from traces a through c. EPR conditions: microwave frequency, 9.41 GHz; modulation amplitude, 10 Gpp; microwave power, 115 mW; $T =$ 11 K. The recording time of each spectrum was 50 s.

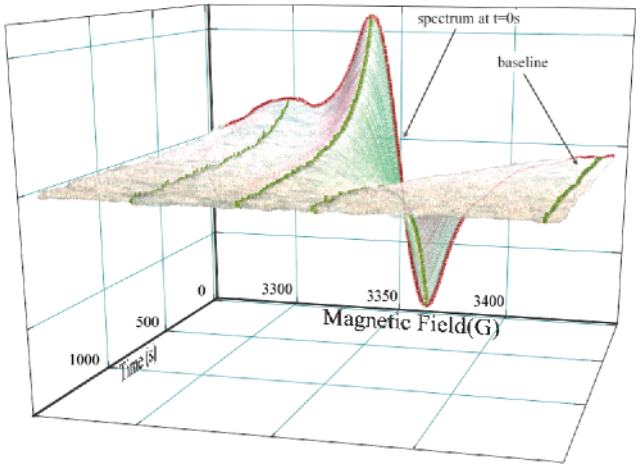

FIGURE 3: Rapid scan spectra of the $(S_1Y_Z)_{vis}$ signal in an ascorbate-treated spinach PSII preparation supplemented with duroquinone. The surface consists of 738 spectra taken every 2 s. The red trace ($t = 0$ s) was recorded 15 s after the flash. The background spectrum obtained after full decay of the $g = 2.035$ component was subtracted from all traces. EPR conditions: $T = 11$ K; microwave frequency, 9.41 GHz; modulation amplitude, 10 Gpp; microwave power, 115 mW; center field = 3350 G; sweep width = 200 G; sweep time = 2 s; time constant = 30 ms.

spectrum. In an earlier study Sigfridson et al. (*27*) reported full spectra decay kinetics for the $(S_1Y_Z^\bullet)_{vis}$ signal by employing conventional slow scans. The results to be presented next are in general agreement with this earlier study, but the use of flash illumination in combination with rapid scans has allowed for the detection of a rapidly decaying component, as detailed below. Figure 3 shows a representative kinetic surface.

In Figure 4(left) we plot the decay of the signal intensity at the low-field side of the $g = 2.035$ component of the $(S_1Y_Z^\bullet)_{vis}$ spectrum along with a single exponential fit. The

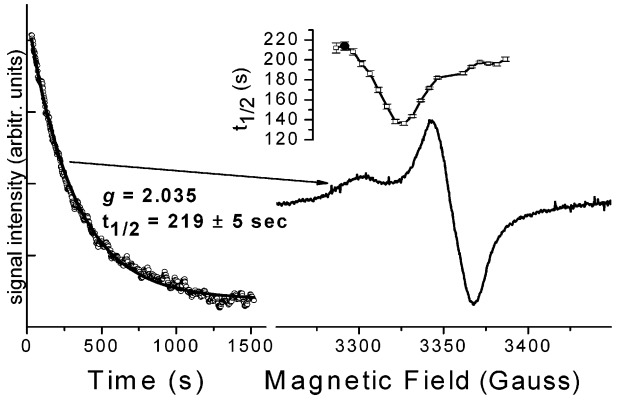

FIGURE 4: Left: Decay kinetics at 11 K of the rising part of the $g = 2.035$ component of the $(S_1Y_Z^\bullet)_{vis}$ spectrum obtained by the use of rapid scans (see Figure 3). Right: Variation of the decay half-time at different field positions across the $(S_1Y_Z^\bullet)_{vis}$ spectrum. The $(S_1Y_Z^\bullet)_{vis}$ spectrum is also included for reference.

latter yields a $t_{1/2}$ of approximately 220 s. A similar computation was done at various magnetic field values across the spectrum, and the resulting $t_{1/2}$ values are plotted as a function of the magnetic field in Figure 4 (right, upper part). The $(S_1Y_Z^\bullet)_{vis}$ spectrum is also included for reference (Figure 4, right, lower part). It is noted that the decay kinetics varies at different parts of the spectrum. The slowest decay, $t_{1/2}$ ca. 220 s, is observed at the rising part of the $g = 2.035$ signal, while the decay becomes significantly faster, $t_{1/2}$ 136 s, around 3325 G. The decay half-time increases again gradually at higher field values but does not quite reach the low-field maximum. This variation in the decay half-time suggests that the $(S_1Y_Z^\bullet)_{vis}$ spectrum is the convolution of at least two components with different decay kinetics. The relative amplitude of the two components across the spectrum modulates the overall $t_{1/2}$ time. To deconvolute the spectrum, the following approach was applied.

A Fast Decaying Component, 26 G Width, of the $(S_1Y_Z^\bullet)_{vis}$ Spectrum. Figure 5 compares the spectrum recorded immediately after the flash, (a), to the spectrum recorded 6.5 min after the flash, (b). The latter has been multiplied by a factor corresponding to the decay kinetics of the rising part of the $g = 2.035$ signal (Figure 4, left). Subtraction of the two spectra reveals a derivative-shaped signal (26 G wide, $g \sim 2$), (c). Signals similar to those of Figure 5 (c) were obtained by subtraction of traces recorded at different times after the flash and in samples with Tyr D oxidized or fully reduced.

The "26 G" component in Figure 5 peaks close to the position where $t_{1/2}$ becomes minimum in Figure 4. Actually, the lowest $t_{1/2}$ value, 136 s, is observed at somewhat lower field values, indicating that at this position the 26 G component has the strongest relative contribution. The 136 s is an upper limit to the decay half-time of the 26 G component. A lower limit was estimated in the following manner. The 220 s decay half-time of the rising part (low-field side) of the $g = 2.035$ signal (Figure 4) was assumed to represent the true decay half-time of this component. This half-time has been used to normalize the spectra at different times to the same $g = 2.035$ intensity and obtain traces of the 26 G component in a manner similar to that of Figure 5. The fitting procedure used, described in Materials and Methods, gives a $t_{1/2}$ of 80 s. This represents a lower limit

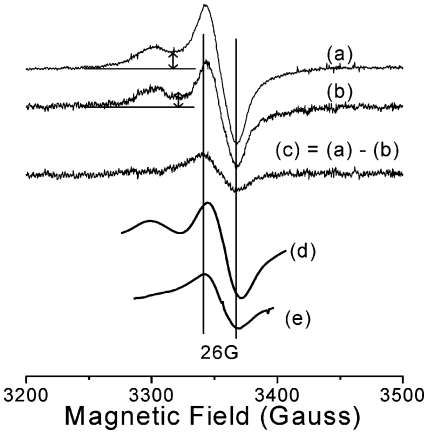

FIGURE 5: Comparison of $(S_1Y_Z^{\bullet})_{vis}$ spectra recorded (a) immediately after visible flash excitation of S_1 and (b) 6.5 min after the flash, normalized to the same $g = 2.035$ size. (c) = (a) − (b) difference spectrum revealing a 26 G component that decays faster than the rest of the spectrum. The background (30 min spectrum) was subtracted from the original spectra prior to normalization. (d, e) Deconvolution of the $(S_1Y_Z^{\bullet})_{vis}$ spectrum into a slow ($t_1 = 275$ s) (d) and a fast ($t_2 = 100$ s) (e) component by simulation of the full spectral surface of Figure 3 (see accompanying text and Materials and Methods for details). Ascorbate-treated spinach PSII samples (+duroquinone) were used in order to eliminate the Tyr $D^{\bullet}$ signal. EPR parameters: microwave frequency, 9.41 GHz; modulation amplitude, 10 Gpp; microwave power, 115 mW; $T =$ 10 K. The recording time of each spectrum was 50 s. EPR parameters for (d) and (e) are those of Figure 3.

to the decay half-time of the 26 G component, since spectra at long times become too noisy when normalized, and the tail of the 26 G signal decay is likely lost in the background. Also, the rising part of the $g = 2.035$ signal may contain weak contributions from the tail of the 26 G component, and this would make the actual half-time of the $g = 2.035$ component somewhat longer than 220 s.

A More Thorough Analysis. The results of the above approximate analysis are refined by fits of the full spectral surface of Figure 3 in magnetic field steps of 2 G (see Materials and Methods). The analysis assumes double exponential kinetics with stable half-time values along the magnetic field axis and variable intensity factors. Conservative estimates of the two half-times obtained from this more thorough analysis are 270 ± 35 and 90 ± 15 s. The uncertainties are due to the extent of overlap of the tail of the 26 G component with the rising part of the $g = 2.035$ signal. This does not alter appreciably the spectral shape of the two components, but it affects the decay rate of the $g =$ 2.035 component. The spectral deconvolution with half-times of 275 and 100 s for the slow and fast component is given in Figure 5 (d and e).

Microwave Power Dependence of the $(S_1Y_Z^{\bullet})_{vis}$ Spectral Components. The $P_{1/2}$ of the $g = 2.035$ component of both the $(S_1Y_Z^{\bullet})_{vis}$ and the $(S_1Y_Z^{\bullet})_{NIR}$ spectrum was determined earlier (*14*). It has a strong temperature dependence with $P_{1/2}$ values of 1.7/11/96 mW at 3.8/7/11 K, respectively. Examination of the power dependence of the 26 G component, resolved by the method of Figure 5, at 11 K indicates a similar power dependence with the $g = 2.035$ signal. The 26 G component corresponds, therefore, to a fast relaxing species, like the $g = 2.035$ component. In addition to the split components of the $(S_1Y_Z^{\bullet})_{vis}$ spectrum small amounts of slowly relaxing narrow components are always present in the spectra, as was mentioned in the beginning of the Results section. At low microwave power, 0.070 mW, a signal II-like component persists, even in ascorbate-treated spinach PSII samples (data not shown). This component has the same decay rate within signal to noise ratio with the $g = 2.035$ signal and was tentatively assigned earlier (*18*) to the interaction of Tyr $Z^{\bullet}$ with the diamagnetic $S = 0$ state of the Mn cluster in S_1.

The 26 G Component Is Assigned to a Heterogeneous $S_1Y_Z^{\bullet}$ Population. The fast decaying 26 G signal has the characteristics of a metalloradical signal, a line width broader than signal II and a high microwave power for saturation ($P_{1/2}$ close to 70 mW at 11 K). Metalloradical signals have been observed in photosystem II from both the acceptor and the donor side. In the acceptor side a good candidate could be $(pheophytin)^{-}$. Split EPR signals attributed to this radical magnetically interacting with the $Q_A^{-}Fe^{2+}$ complex have been studied earlier (*28*, *29*). The present case would correspond to the configuration $(pheo)^{-}Q_AFe^{2+}$ that has never been trapped before by EPR spectroscopy. This assignment would be compatible with the absence of the fast decaying signal in the $(S_1Y_Z^{\bullet})_{NIR}$ spectrum since no charge separation takes place in this case (see, however, ref *30*). The decay rate (~110 s) seems, however, much too slow compared with the $pheo^{-}$ to Q_A electron transfer rate. Also, experiments in samples with the non-heme iron preoxidized (not shown) yielded no discernible changes in the 26 G component signal shape despite the change in the spin of the iron from $S = 2$ to $S = {}^5/_2$. The most reasonable assumption therefore is that the 26 G signal results from the interaction of Tyr $Z^{\bullet}$ with a modified configuration of the Mn cluster in S_1. The $g =$ 2.035 signal appears to be associated with a configuration of S_1 that corresponds to the S_2 configuration yielding the multiline signal since, during NIR excitation of the S_2 state, only the multiline form shows sensitivity (unpublished observations) and converts to the $(S_1Y_Z^{\bullet})_{NIR}$ transient characterized by the $g = 2.035$ signal. The 26 G component could accordingly be assigned to S_1 centers that advance to the g = 4.1 signal during the S_1 to S_2 transition. Evidence supporting the above assignments is obtained by the following experiments.

Correlation of the $g = 2.035$ and the 26 G Components of the $(S_1Y_Z^{\bullet})_{vis}$ Signal with the Multiline and the $g = 4.1$ Conformations of the S_2 State. (a) Advancement of the $(S_1Y_Z^{\bullet})_{vis}$ Intermediate to S_2 at Elevated Temperatures. The fact that the $(S_1Y_Z^{\bullet})_{vis}$ intermediate advances to S_2 at 77 K has been demonstrated by Nugent et al. (*13*). In the present experiments we have examined the amount and composition of the S_2-state signal obtained by rapid transfer of the $(S_1Y_Z^{\bullet})_{vis}$ intermediate to ca. 200 K. Figure 6 compares the S_2-state spectra obtained as follows: (A) flash illumination at 11 K to prepare $(S_1Y_Z^{\bullet})_{vis}$ and immediate dark incubation at 200 K for 1.5 min; (B) flash illumination at 11 K, 7 min dark incubation at 11 K to allow for the decay of the 26 G component, and 1.5 min dark incubation at 200 K. The accumulated effect of two (Figure 6A) or five (Figure 6B) such cycles, respectively, is shown. The spectra are compared with the maximum S_2-state spectrum obtained in the same samples by continuous illumination at 200 K (at the end of the experiments). The latter has been scaled down by the indicated factors to match the multiline part of the spectrum. The following observations can be made: significant amounts

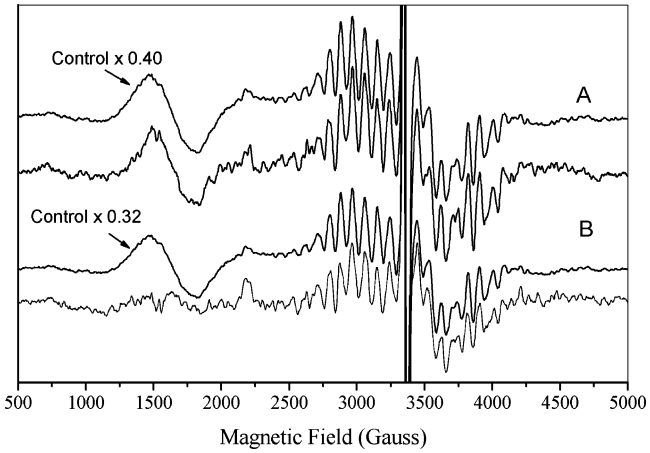

FIGURE 6: S_2-state spectra obtained after 1.5 min incubation at 200 K of samples that were prepared in the $(S_1Y_Z^\bullet)_{vis}$ at 11 K and were transferred either immediately to 200 K or after a 7 min incubation period at 11 K. The accumulated effect of two or five such cycles, respectively, is shown. The spectra are compared with the maximum S_2-state spectrum obtained in the same sample (at the end of the experiments) by continuous illumination at 200 K. The latter has been scaled down by the indicated factors. EPR conditions: modulation amplitude, 25 G; power, 57 mW; time constant, 100 ms; $T = 11$ K.

of the multiline spectrum are formed. Following the two cycles of immediate transfer to 200 K, 40% of the centers advance to the S_2 state, while additional cycles (data not shown) result in S_2 populations exceeding 50%. This indicates that the majority of centers can produce the $(S_1Y_Z^\bullet)_{vis}$ intermediate at liquid helium temperatures (see also ref *16*). Interestingly enough, the relative amount of the $g = 4.1$ signal formed in Figure 6B is vanishingly small. This correlates nicely with the fact that the 26 G component decays almost fully after 7 min of incubation at 11 K.

Figure 6 suggests also a correlation between the size of the $g = 2.035$ signal and the amount of the multiline signal obtained by transfer to 200 K. In the sample that was incubated for 7 min at 11 K before transfer to 200 K, the multiline signal is significantly smaller, if one corrects for the larger number of cycles in this experiment. To obtain a more accurate correlation, the amount of the $g = 2.035$ signal that remains following various delay times at 11 K after the flash was compared with the amount of multiline signal obtained by subsequent transfer to 200 K (Figure 7). A linear correlation is found within experimental error. This result, together with the approximate correlation between the 26 G signal and the $g = 4.1$ S_2 component in Figure 6, provides strong experimental support to the assignment of the "$g = 2.035$" and the 26 G components of the $(S_1Y_Z^\bullet)_{vis}$ EPR signal as precursors of the "multiline" and "$g = 4.1$" components of the S_2 state, respectively. Additional support is provided by the following experiments where sucrose is replaced by glycerol as a cryoprotectant.

(b) The $(S_1Y_Z^\bullet)_{vis}$ Signal in Preparations That Exhibit Vanishing or Very Small Amounts of the $g = 4.1$ S_2-State Signal. Thermophilic, cyanobacterial preparations do not generally exhibit the $g = 4.1$ component in the S_2-state spectra (*31*; see also refs *14* and *32*). The $(S_1Y_Z^\bullet)_{vis}$ in *S. elongatus* or *Synechococcus vulcanus* preparations is very similar to the $(S_1Y_Z^\bullet)_{NIR}$ spectrum in Figure 2c except for a small narrow contribution at $g = 2.0$ due presumably to free radical side donors (spectra not shown). No evidence

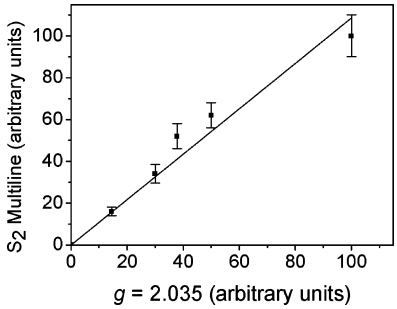

FIGURE 7: The amount of S_2 multiline formed as a function of the size of the precursor $g = 2.035$ signal. A sample was flash illuminated at 11 K to form the $(S_1Y_Z^\bullet)_{vis}$ intermediate, and following a variable delay time (in the range of the decay time of the $g = 2.035$ signal in Figure 4) it was incubated at 200 K for 1.5 min before recording the multiline spectrum at 11 K. The sample was then allowed to decay to the S_1 state by incubation at 0 °C for 50 min, and the cycle was repeated for a different delay time at 11 K. The sample contained 1 mM PPBQ.

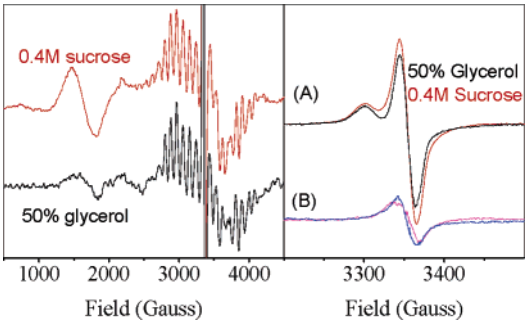

FIGURE 8: Comparison of the EPR spectra of a sample containing sucrose (typical of the samples used in this study) with a sample where the sucrose is replaced with 50% (v/v) glycerol. Left panel: S_2 minus S_1 difference spectra. The spectra have been normalized to approximately the same intensity of the multiline signal, and the same normalization factor was used in the right panel. Right panel: (A) superposition of the $(S_1Y_Z^\bullet)_{vis}$ spectra obtained as in Figure 1A, lowest trace; (B) difference (red − black trace) of the two spectra in (A) (magenta trace); the 26 G signal obtained as in Figure 5 in the sucrose sample (blue trace). EPR conditions: $T = 11$ K; modulation amplitude, 25 G (left panel) or 10 G (right panel); microwave power, 50 mW. The samples contained 1 mM duroquinone.

whatsoever could be detected in the spectra for the 26 G component.

Glycerol is often used as a cryoprotectant in PSII preparations. Its presence does not appear to alter the EPR spectra of the OEC or the NIR sensitivity of the S_2 and S_3 states except that it reduces heterogeneity. The $g = 4.1$ component of the S_2-state spectrum has an intensity much smaller than the multiline signal in samples containing glycerol instead of sucrose (*33*). This is apparent by a comparison of the S_2-state spectra (Figure 8, left panel) in two samples: a control sample containing 0.4 M sucrose and a sample where sucrose is replaced with 50% (v/v) glycerol. The spectra have been scaled to the same multiline intensity. Clearly, the $g = 4.1$ contribution is much smaller in the glycerol-treated sample, representing about 25% of the size observed in the control sample. The right panel of Figure 8 compares the $(S_1Y_Z^\bullet)_{vis}$ spectra in the two kinds of samples using the same normalization factor used in the left panel. Differences in the $g = 2$ region can be observed. Subtraction of the two spectra (sucrose minus glycerol sample) yields a trace (magenta colored) which closely resembles the spectrum of

the 26 G component (blue trace). The latter was obtained as in Figure 5c in the sucrose sample. Actually, the spectrum of the glycerol sample resembles that of the sucrose sample recorded 7 min after the flash excitation (spectrum not shown), apart from small differences in the $g = 2.0$ region. In a separate experiment the presence of a fast decaying component in the $(S_1Y_Z^{\bullet})_{vis}$ spectrum of the glycerol-containing sample was investigated. A small 26 G component, representing less than 30% of the magenta trace of Figure 8(B), could be detected (data not shown) by an experiment similar to that of Figure 5. Therefore, both the $g = 4.1$ component in the S_2 spectrum and the fast component in the $(S_1Y_Z^{\bullet})_{vis}$ spectrum are significantly smaller in the glycerol-containing samples.

Implications about Heterogeneity in S_1 and Mn Valence Assignments. The present results show that the heterogeneity observed in the S_2-state EPR spectra is also present in the $(S_1Y_Z^{\bullet})_{vis}$ spectrum. As the latter is produced at liquid helium temperatures, at which molecular motions are inhibited, this heterogeneity must be already present in S_1. Two different kinds of EPR signals at parallel mode have been reported for the S_1 state: a broad signal at $g = 4.8$ (*10*, *11*) and a multiline signal at $g = 12$ (*12*). To the best of our knowledge no one has reported the simultaneous detection of both signals in the same preparation. The $g = 4.8$ signal is observed in spinach BBY preparations, while the $g = 12$ multiline signal has been detected in *Synechocystis* (a cyanobacterium exhibiting significant differences from the thermophilic cyanobacteria of the present study) or in spinach BBY preparations after removal of the 23 and 17 kDa extrinsic proteins. The underlying difficulty with the S_1 studies is that S_1 is an integer spin state and is therefore difficult to probe by EPR spectroscopy. The observation of only one type of EPR signal does not mean that this is the only signal present in S_1.

The relatively recent advances in the determination of the 3-D structure of PSII by X-ray crystallography (*34*−*37*) in combination with spectroscopy (see, e.g., reviews in refs *1*−*3* and *38*) and mutation and FTIR work (see, e.g., reviews in refs *39* and *40*) allow tentative valence assignments to the individual Mn ions constituting the Mn cluster. In a recent paper (*9*) the following Mn valence distribution in S_2 was suggested: ^{1}Mn(III)−^{2}Mn(IV)−^{3,4}Mn(IV) for the conformation that gives rise to the multiline EPR signal and ^{1}Mn(IV)−^{2}Mn(III)−^{3,4}Mn(IV) for the conformation giving the $g = 4.1$ signal. ^{1,2}Mn(III)−^{3,4}Mn(IV) is the S_1 conformation which advances to the S_2 multiline and, therefore, the conformation that gives rise to the $g = 2.035$ component of the $(S_1Y_Z^{\bullet})_{vis}$ spectrum. Assuming that the S_1 configuration producing the 26 G $(S_1Y_Z^{\bullet})_{vis}$ component has a different valence distribution, then this probably is ^{1}Mn(IV)−^{2}Mn(III)−^{3}Mn(III)−^{4}Mn(IV). The latter is the only option left, if one combines the observations that ^{4}Mn is ligated by aspartate-170 of the D1 polypeptide (*37*) and according to FTIR studies is not oxidized during the S-state transitions (*41*). The altered spin distribution of the Mn cluster in this case would explain the different $(S_1Y_Z^{\bullet})_{vis}$ spectrum. The more positive charge (the higher valence) on ^{1}Mn could indirectly raise the p*K* of His 190 and in turn the reduction potential of Tyr Z$^{\bullet}$ resulting in a faster recombination rate, as is experimentally observed. The tentative model of Figure 9 and the valence assignments indicating that ^{1}Mn is not oxidized during the S_1 to S_2 and the S_2 to S_3 (*9*) transitions are not incompatible with recent FTIR results on D_1-E189 mutants (*42*), which suggest that if D_1-E189 is a ligand to Mn, then this Mn ion does not undergo oxidation during any of the transitions from S_0 to S_3. It should be noted that samples used in the FTIR experiments usually contain glycerol. As glycerol removes the heterogeneous S_1 (26 G component) and S_2 ($g = 4.1$) populations, the respective FTIR results can be related only to the $g = 2.035$ $(S_1Y_Z^{\bullet})$ and the multiline S_2 conformations.

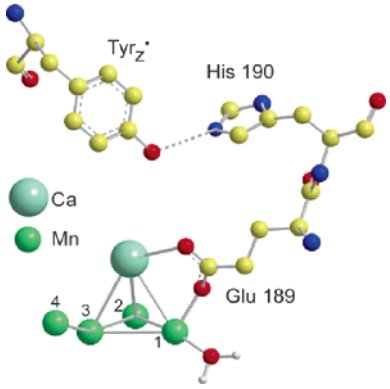

FIGURE 9: A tentative molecular model based on the most recent crystallographic results (*37*; see also ref *9*), showing the arrangement of the Mn cluster in S_1 and the connection to the Tyr Z. Valence assignments of the Mn ions in the two heterogeneous S_1 populations are discussed in the text.

Summary of Main Observations and Conclusions. (i) The intermediate trapped by illumination of the S_1 state at liquid helium temperatures, $(S_1Y_Z^{\bullet})_{vis}$, is heterogeneous in nature and contains two kinetically and spectroscopically distinct metalloradical components: (a) a slowly decaying component ($t_{1/2} = 270 \pm 35$ s at 11 K) with a spectrum resembling that of the $(S_1Y_Z^{\bullet})_{NIR}$ intermediate (i.e., the signal produced by NIR excitation of S_2 with the characteristic contribution at $g = 2.035$) and (b) a fast decaying ($t_{1/2} = 90 \pm 15$ s) derivative-shaped, 26 G width, component. (ii) A few cycles of illumination at 11 K [to produce the $(S_1Y_Z^{\bullet})_{vis}$ intermediate] followed by immediate transfer in the dark to 200 K result in the accumulation of more than 50% of the S_2 state; the majority of centers is accordingly capable of producing the $(S_1Y_Z^{\bullet})_{vis}$ intermediate at 11 K. (iii) The slow and the fast decaying components of the $(S_1Y_Z^{\bullet})_{vis}$ intermediate are the precursors of the multiline and the $g = 4.1$ conformations of S_2, respectively; the heterogeneity observed in S_2 is therefore already present in S_1. (iv) The combination of recent observations allows the tentative assignment of specific valences to the Mn ions in the two heterogeneous conformations of S_1 and S_2.

REFERENCES

1. Goussias, C., Boussac, A., and Rutherford, A. W. (2002) Photosystem II and photosynthetic oxidation of water: an overview, *Philos. Trans. R. Soc., Ser. B 357*, 1369−1381.
2. Yachandra, V. K. (2005) The catalytic manganese cluster: organization of the metal ions, *in Photosystem II: The Water/Plastoquinone Oxido-Reductase of Photosynthesis* (Wydrzynski, T., and Satoh, K., Eds.) pp 235−260, Kluwer Academic Publishers, Dordrecht, The Netherlands.
3. Hillier, W., and Messinger, J. (2005) Mechanism of photosynthetic oxygen production, *in Photosystem II: The Water/Plastoquinone Oxido-Reductase of Photosynthesis* (Wydrzynski, T., and Satoh,

K., Eds.) pp 567−608, Kluwer Academic Publishers, Dordrecht, The Netherlands.
4. Dismukes, G. C., and Siderer, Y. (1981) Intermediates of a polynuclear center involved in photosynthetic oxidation of water, *Proc. Natl. Acad. Sci. U.S.A. 78*, 274−278.
5. Casey, J., and Sauer, K. (1984) EPR detection of a cryogenically photogenerated intermediate in photosynthetic oxygen evolution, *Biochim. Biophys. Acta 767*, 21−28.
6. Zimmermann, J. L., and Rutherford, A. W. (1984) EPR studies ofthe oxygen evoIving enzyme of photosystem II, *Biochim. Biophys. Acta 767*, 160−167.
7. Boussac, A., and Rutherford, A. W. (2000) Comparative study of the $g = 4.1$ EPR signals in the S_2 state of photosystem II, *Biochim. Biophys. Acta 1457*, 145−156.
8. Peloquin, J. M., Campbell, K. A., Randall, D. W., Evanchik, M. A., Pecoraro, V. L., Armstrong, W. H., and Britt, R. D. (2000) ^{55}Mn ENDOR of the S_2-state multiline EPR signal of photosystem II: Implications *o*n the structure of the tetranuclear Mn cluster, *J. Am. Chem. Soc. 122*, 10926−10942.
9. Ioannidis, N., Zahariou, G., and Petrouleas, V. (2006) Trapping of the S_2 to S_3 state intermediate of the oxygen evolving complex of photosystem II, *Biochemistry 45*, 6252−6259.
10. Dexheimer, S. L., and Klein, M. P. (1992) Detection of a paramagnetic intermediate in the S_1-state of the photosynthetic oxygen-evolving complex, *J. Am. Chem. Soc. 114*, 2821−2826.
11. Yamauchi, T., Mino, H., Matsukawa, T., Kawamori, A., and Ono, T. (1997) Parallel polarization electron paramagnetic resonance studies of the S_1-state manganese cluster in the photosynthetic oxygen-evolving system, *Biochemistry 36*, 7520−7526.
12. Campbell, K. A., Gregor, W., Pham, D. P., Peloquin, J. M., Debus, R. J., and Britt, R. D. (1998) The 23 and 17 kDa extrinsic proteins of photosystem II modulate the magnetic properties of the S_1-state manganese cluster, *Biochemistry 37*, 5039−5045.
13. Nugent, J. H. A., Muhiuddin, I. P., and Evans, M. C. W. (2002) Electron transfer from the water oxidizing complex at cryogenic temperatures: The S_1 to S_2 step, *Biochemistry 41*, 4117−4126.
14. Koulougliotis, D., Shen, J. R., Ioannidis, N., and Petrouleas, V. (2003) Near-IR irradiation of the S_2 state of the water oxidizing complex of photosystem II at liquid helium temperatures produces the metalloradical intermediate attributed to $S_1Y_Z^{\bullet}$, *Biochemistry 42*, 3045−3053.
15. Zhang, C. X., and Styring, S. (2003) Formation of split electron paramagnetic resonance signals in photosystem II suggests that tyrosine(z) can be photooxidized at 5 K in the S_0 and S_1 states of the oxygen-evolving complex, *Biochemistry 42*, 8066−8076.
16. Zhang, C. X., Boussac, A., and Rutherford, A. W. (2004) Low-temperature electron transfer in photosystem II: A tyrosyl radical and semiquinone charge pair, *Biochemistry 43*, 13787−13795.
17. Ioannidis, N., Nugent, J. H. A., and Petrouleas, V. (2002) Intermediates of the S_3 state of the oxygen-evolving complex of photosystem II, *Biochemistry 41*, 9589−9600.
18. Koulougliotis, D., Teutlolf, C., Sanakis, Y., Lubitz, W., and Petrouleas, V. (2004) The $S_1Y_Z^{\bullet}$ metalloradical intermediate in photosystem II: an X- and W-band EPR study, *Phys. Chem. Chem. Phys. 6*, 4859−4863.
19. Su, J.-H., Havelius, K. G. V., Mamedov, F., Ho, F. M., and Styring, S. (2006) Split EPR signals from photosystem II are modified by methanol, reflecting S state-dependent binding and alterations in the magnetic coupling in the CaMn4 cluster, *Biochemistry 45*, 7617−7627.
20. Petrouleas, V., Koulougliotis, D., and Ioannidis, N. (2005) Trapping of metalloradical intermediates of the S-states at liquid helium temperatures. Overview of the phenomenology and mechanistic implications, *Biochemistry 44*, 6723−6728.
21. Berthold, D. A., Babcock, G. T., and Yocum, C. F. (1981) A highly resolved, oxygen-evolving photosystem-II preparation from spinach thylakoid membranes—Electron-paramagnetic-resonance and electron-transport properties, *FEBS Lett. 134*, 231−234.
22. Ford, R. C., and Evans, M. C. W. (1983) Isolation of a photosystem-2 preparation from higher-plants with highly enriched oxygen evolution activity, *FEBS Lett. 160*, 159−164.
23. Faller, P., Pascal, A., and Rutherford, A. W. (2001) Beta-carotene redox reactions in photosystem II: Electron transfer pathway, *Biochemistry 40*, 6431−6440.
24. Boussac, A., and Rutherford, A. W. (1995) Does the formation of the S_3-state in Ca^{2+}-depleted photosystem-II correspond to an oxidation of tyrosine-Z detectable by CW-EPR at room-temperature?, *Biochim. Biophys. Acta 1230*, 195−201.
25. Petrouleas, V., and Diner, B. A. (1990) Formation by NO of nitrosyl adducts of redox components of the photosystem-II reaction center. I. NO binds to the acceptor-side non-heme iron, *Biochim. Biophys. Acta 1015*, 131−140.
26. Szalai, V. A., and Brudvig, G. W. (1996) Reversible binding of nitric oxide to tyrosyl radicals in photosystem II. Nitric oxide quenches formation of the S_3 EPR signal species in acetate-inhibited photosystem II, *Biochemistry 35*, 15080−15087.
27. Sigfridsson, K. G. V., Su, J.-H., Feyziyev, Y., and Styring, S. (2005) The spectral resolution of the "Split S1" and "Split S0" EPR-signals from photosystem II induced by illumination at 5 K, in *Photosynthesis: Aspects to Global Perspectives* (van der Est, A., and Bruce, D., Eds.) pp 386−388, Alliance Communications Group, Lawrence, KS.
28. Klimov, V. V., Dolan, E., Shaw, E. R., and Ke, B. (1980) Interaction between the intermediary electron-acceptor (pheophytin) and a possible plastoquinone-iron complex in photosystem-II reaction centers, *Proc. Natl. Acad. Sci. U.S.A. 77*, 7227−7231.
29. Deligiannakis, Y., and Rutherford, A. W. (1996) Spin-lattice relaxation of the pheophytin, $Pheo^{-}$, radical of photosystem II, *Biochemistry 35*, 11239−11246.
30. Hughes, J. L., Smith, P., Pace, R., and Krausz, E. (2006) Charge separation in photosystem II core complexes induced by 690−730 nm excitation at 1.7 K, *Biochim. Biophys. Acta 1757*, 841−851.
31. McDermott, A. E., Yachandra, V. K., Guiles, R. D., Cole, J. L., Dexheimer, S. L., Britt, R. D., Sauer, K., and Klein, M. P. (1988) Characterization of the manganese O_2-evolving complex and the iron-quinone acceptor complex in photosystem II from a thermophilic cyanobacterium by electron paramagnetic resonance and X-ray absorption spectroscopy, *Biochemistry 27*, 4021−4031.
32. Boussac, A., Kuhl, H., Un, S., Rogner, M. and Rutherford A. W. (1998) Effect of near-infrared light on the S2-state of the manganese complex of photosystem II from *Synechococcus elongatus*, *Biochemistry 37*, 8995−9000.
33. Zimmermann, J. L., and Rutherford, A. W. (1986) Electron paramagnetic resonance properties of the S2 state of the oxygen evoIving compIex of photosystem II, *Biochemistry 25*, 4609−4615.
34. Zouni, A., Witt, H. T., Kern, J., Fromme, P., Krauss, N., Saenger, W., and Orth, P. (2001) Crystal structure of photosystem II from *Synechococcus elongatus* at 3.8 Å resolution, *Nature 409*, 739−743.
35. Kamiya, N., and Shen, J. R. (2003) Crystal structure of oxygen-evolving photosystem II from *Thermosynechococcus vulcanus* at 3.7-Å resolution, *Proc. Natl. Acad. Sci. U.S.A. 100*, 98−103.
36. Ferreira, K. N., Iverson, T. M., Maghlaoui, K., Barber, J., and Iwata, S. (2004) Architecture of the photosynthetic oxygen-evolving center, *Science 303*, 1831−1838.
37. Loll, B., Kern, J., Saenger, W., Zouni, A., and Biesiadka, J. (2005) Towards complete cofactor arrangement in the 3.0 Å resolution structure of photosystem II, *Nat. Lett. 438*, 1040−1044.
38. Dau, H., Iuzzolino, I., and Dittmer, J. (2001) The tetra-manganese complex *o*f photosystem II during its redox cycle-X-ray absorption results and mechanistic implications, *Biochim. Biophys. Acta 1503*, 24−39.
39. Debus, R. (2005) The catalytic manganese cluster: protein ligation, in *Photosystem II. The Light Driven Water:Plastiquinone Oxidoreductase* (Wydrzynski, T., and Satoh, K., Eds.) pp 261−284, Springer, Dordrecht, The Netherlands.
40. Noguchi, T., and Berthomieu, C. (2005) Molecular analysis by vibrational spectroscopy, in *Photosystem II. The Light Driven Water:Plastiquinone Oxidoreductase* (Wydrzynski, T., and Satoh, K., Eds.) pp 367−387, Springer, Dordrecht, The Netherlands.
41. Debus, R. J., Strickler, M. A., Walker, L. M., and Hillier, W. (2005) N*o* evidence from FTIR difference spectroscopy that aspartate 170 *o*f the D1 polypeptide ligates a manganese ion that undergoes oxidation during the S_0 to S_1, S_1 to S_2, or S_2 to S_3 transitions in photosystem II, *Biochemistry 44*, 1367−1374.
42. Strickler, M. A., Hillier, W., and Debus, R. J. (2006) No evidence from FTIR difference spectroscopy that glutamate-189 of the D1 polypeptide ligates a Mn ion that undergoes oxidation during the S_0 to S_1, S_1 to S_2, or S_2 to S_3 transitions in photosystem II, *Biochemistry 45*, 8801−8811.

BI061224I